Available online at www.sciencedirect.com
SCIENCE DIRECT
Nuclear Instruments and Methods in Physics Research A 561 (2006) 230–236
NUCLEAR INSTRUMENTS & METHODS IN PHYSICS RESEARCH Section A
www.elsevier.com/locate/nima

Chaotic dynamics and halo formation in charged-particle beams

C.L. Bohn*, G.T. Betzel, I.V. Sideris

Beam Physics and Astrophysics Group, Department of Physics, Northern Illinois University, DeKalb, IL 60115, USA

Available online 10 February 2006

Abstract

An old problem, but a new area of fundamental research, is characterizing orbital dynamics and its consequences in time-dependent potentials. Regarding nonequilibrium space-charge potentials, one clear consequence is halo formation. We show that orbital chaos normally plays a central role in halo formation. In turn, the ability to quantify chaos is centrally important. We show examples of the generation and consequences of chaos in nonequilibrium beams, and we apply a newly developed tool for pinpointing orbital chaos in time-dependent potentials.

PACS: 45.10.−b; 52.25.Fi; 29.27.−a; 05.45.−a

Keywords: Beam halo; Chaos; Nonequilibrium beams

1. Introduction

Although detailed microscopic dynamics has been studied and characterized in representative time-independent and time-dependent space-charge potentials [1,2], much remains to be learned, especially regarding how microscopic evolution drives the macroscopic properties of the charged-particle beam. The beam can be viewed unequivocally as a collection of N orbits. That Liouville's Theorem applies rigorously in the respective $6N$-dimensional phase space is not especially helpful computationally. Instead, one normally appeals to the BBGKY hierarchy of s-particle reduced distribution functions ($s \leqslant N$), decomposes these reduced distribution functions into a hierarchy of correlation functions, and then appeals optimistically to time-scale arguments to truncate this hierarchy. The end result is, to lowest order, the Vlasov equation, and to next order, the Landau kinetic equation [3]. In either case one has an equation for the evolution of the distribution function $f(\mathbf{x}, \mathbf{p}, t)$ of particles in the 6-dimensional phase space $(\mathbf{x}, \mathbf{p})$ of a single particle. Yet, to do this, one in fact sacrifices some of the physics, usually by arguing that orbits quickly 'forget' their initial conditions so that their mutual interactions in effect constitute a Markov process. One major consequence of this argument is that Liouville's Theorem in general will *not* apply rigorously to the 6-dimensional phase space. For example, the Landau kinetic equation explicitly folds in a non-Liouvillian 'collision term' that enables internal free energy eventually to thermalize. From a practical point of view, this means the volume of phase space subtended by the N particles tends to grow.

In this paper, we adopt the Vlasov–Poisson–Maxwell picture. We take the density and potential to be smooth (coarse-grained), and we regard individual particles to move in response to this globally smooth potential. In other words, we assume that the 'continuum limit' is valid, although it has been shown for beams that this is not necessarily true [4]. However, our interest here is to isolate the importance of time dependence for the evolution of a beam bunch; we thus purposely avoid any other complication inherent to a real beam. In particular, our emphasis is on dynamical chaos arising from coarse-grained forces; we purposely suppress microscopic, stochastic chaos arising from granularity associated with discrete particles. As will be demonstrated, time dependence alone can trigger complicated evolutionary dynamics, including dynamical chaos. How the dynamics drives the macroscopic properties of the beam can readily be understood in terms of

*Corresponding author.
E-mail address: clbohn@fnal.gov (C.L. Bohn).

0168-9002/$ - see front matter © 2006 Elsevier B.V. All rights reserved.
doi:10.1016/j.nima.2006.01.034

mixing, and the qualitative behavior of this mixing depends critically and unequivocally on the nature of the orbits, i.e., whether they are regular or chaotic.

Our treatment will center on a spherically symmetric, homologously breathing, space-charge-dominated beam bunch in the spirit of the 'particle-core model' [5]. Okamoto and Ikegami previously treated a cylindrical version of this model [6], and their work is partial motivation for our investigation. One question we ask is: How does the time dependence influence the population of chaotic orbits? The static beam has zero chaotic orbits because the equation of particle motion is integrable up to quadrature. This is generally not true once the bunch is set into oscillation. We exemplify how the resultant population of chaotic orbits evolves to build a halo. Another question is: Can the presence of colored noise contribute to halo formation? This noise is unavoidable in real machines; hardware and field irregularities will self-consistently influence the space-charge potential and hence the particle orbits. The noise thereby does work on the beam, causing emittance growth and halo formation. For a homologously breathing cylindrical KV beam, the outer KAM tori are robust; modest noise strength will not break them, although they become much more fragile if internal collective modes are excited [2]. Herein we consider only a breathing spherical waterbag beam; there are no internal modes. We again find the outer KAM tori to be robust; however, we also find that, for certain parameter choices, modest colored noise can nonetheless make a big difference in the macroscopic properties of the bunch, to include triggering halo formation where otherwise there would be none. Finally, we apply a new method, which is based on dynamics alone, for efficiently characterizing orbits and orbital intermittency in time-dependent potentials.

2. Spherical waterbag model

The spherical waterbag is comprised of radial orbits. It mimics a spherical beam bunch under the influence of a linear focusing force and an internal repulsive space-charge force [7]. Its equilibrium potential derives from a distribution function $g(r,p) \propto [H_0 - H(r,p)]^{-1/2}$ for $H < H_0$; g is zero otherwise, and H_0 is a constant. The density $\rho(r)$ for a bunch of total charge Q (found by integrating $g(r,p)$ over momentum space) and the total potential $V(r)$ (the sum of the quadratic external focusing potential and the space-charge potential found by solving Poisson's equation) are

$$\rho = \frac{3Q}{4\pi R^3 v}\left\{1 - \frac{i_0[r/(R\alpha)]}{i_0(\xi)}\right\}, \tag{1}$$

$$\begin{aligned} V = {} & \left\{\frac{v}{\xi R\alpha} - \frac{1}{2}\left(1 - \frac{1}{R^3}\right)[(\xi R\alpha)^2 - r^2]\right. \\ & \left. - \frac{\mu}{R} d_0\left(\frac{r}{R\alpha}\right)\right\}\Theta(\xi R\alpha - r) \\ & - \left\{\frac{1}{2}[(\xi R\alpha)^2 - r^2] - \frac{v}{r}\right\}\Theta(r - \xi R\alpha), \end{aligned} \tag{2}$$

wherein $\Theta(y)$ is the Heaviside step function. Auxiliary quantities in these expressions are

$$i_0(y) \equiv y^{-1}\sinh y, \quad d_0(y) \equiv i_0(\xi) - i_0(y)$$

$$\alpha \equiv \left\{\frac{(3+\xi^2)i_0(\xi) - 3\cosh\xi}{[\xi^4 + 15(2+\xi^2)]i_0(\xi) - 5(6+\xi^2)\cosh\xi}\right\}^{1/2}$$

$$\mu \equiv 3\alpha^2/i_0(\xi)$$

$$v \equiv [\xi\alpha^3/i_0(\xi)][(3+\xi^2)i_0(\xi) - 3\cosh\xi]$$

in which the intermediary parameter ξ is found from the space-charge tune depression η by solving

$$\frac{15}{4i_0(\xi)}\frac{(12+5\xi^2)i_0^2(\xi) - 3[3i_0(\xi) + \cosh\xi]\cosh\xi}{[30 + \xi^2(15+\xi^2)]i_0(\xi) - 5(6+\xi^2)\cosh\xi} = \eta^2$$

and R is the 'core radius' (which differs from the actual boundary of the waterbag located at $r = \xi R\alpha$).

By populating the sphere with test particles and letting it oscillate homologously, one has a 'particle-core model' [5] with a nonuniform density that establishes a nonlinear space-charge force on the test particles. This is accomplished by letting R be a function of time determined by the dimensionless 'envelope equation'

$$\ddot{R} + R - \frac{\eta^2}{R^3} - \frac{1-\eta^2}{R^2} = 0, \quad R(0) = M, \ \dot{R}(0) = 0. \tag{3}$$

The length scale is the equilibrium core radius, the time scale is the inverse of the angular external focusing frequency, and M is the 'mismatch'. Thus, the waterbag comprises a two-parameter (η, M) family of models. Due to spherical symmetry, radial motion along every diameter is the same. Accordingly, we take each test particle to be confined to the x-axis; thus, the equation of motion is $\ddot{x} = -\partial_x V$, or, more explicitly

$$\begin{aligned} \ddot{x} + x = {} & \left\{\frac{x}{R^3} - \frac{\mu}{Rx}\left[\cosh\left(\frac{x}{R\alpha}\right) - i_0\left(\frac{x}{R\alpha}\right)\right]\right\}\Theta(\xi R\alpha - |x|) \\ & + v\frac{|x|}{x^3}\Theta(|x| - \xi R\alpha), \quad x(0) = x_0, \ \dot{x}(0) = 0. \end{aligned} \tag{4}$$

In doing so, we have assigned zero angular momentum to all of the test particles. This is a simplification to keep their motion one dimensional; however, in past work [2] we found that the inclusion of orbital angular momentum has no statistically significant impact on, e.g., halo formation.

The major disadvantage of the spherical waterbag model is that, although the equilibrium distribution is self-consistently defined, the homologous oscillation is not self-consistent. Rather, one would expect considerably more complicated evolution. However, the model offers several attractive advantages: (i) the distribution function, the charge density, and the total potential are all analytic; (ii) the tune η parameterizes the family of models, so one can readily explore the range from zero space charge ($\eta = 1$) to the space-charge limit $\eta = 0$; and (iii) whereas all stationary waterbags are integrable in keeping with their spherical symmetry, chaotic orbits arise once they are made

to breathe. This (manifestly deterministic) chaos is thereby fully attributable to the time dependence alone. Thus, this family of models is ideal not only for answering basic questions such as how time dependence triggers chaoticity, but also for highlighting the efficacy of new techniques for quantifying this chaos and for analyzing nonlinear dynamics in general. It is for these reasons that we adopt it.

3. Mixing experiments

The underlying objective of a mixing experiment is to ascertain which points of phase space correspond to chaotic motion vs. regular motion. Suppose, at $t = 0$, we select a point in phase space. We place a test particle at that point and integrate the equation of motion to compute its orbit. We then go to a neighboring point in phase space, one that lies a small distance $|\delta Z| = (|\delta\mathbf{x}|^2 + |\delta\mathbf{p}|^2)^{1/2}$ away from the first point, and redo the procedure. The two orbits will, of course, separate from each other. If the separation is exponential in time, then this phase-space point (of size $|\delta Z|$) is chaotic. If the separation scales as a power of time, then it is regular. This is the basic idea underlying the definition of the Lyapunov exponent λ:

$$\lambda = \lim_{t\to\infty}\left\{\frac{1}{t}\lim_{\delta Z(0)\to 0}\left[\ln\frac{|\delta Z(t)|}{|\delta Z(0)|}\right]\right\}. \tag{5}$$

Note that formally an infinite integration time is required; the standard Lyapunov exponent is a time-averaged quantity. Lyapunov exponents computed from Eq. (5) for the waterbag with $M = 0.5$ and $\eta = 0.15$ are plotted in Fig. 1.

To have confidence in a labeling scheme like this, one wants to have much more statistics than just two orbits provide. Suppose, instead, we take an initially localized 'clump' of, say, 1000 test particles. At $t = 0$ we place all of these test particles within a tiny volume of phase space. We

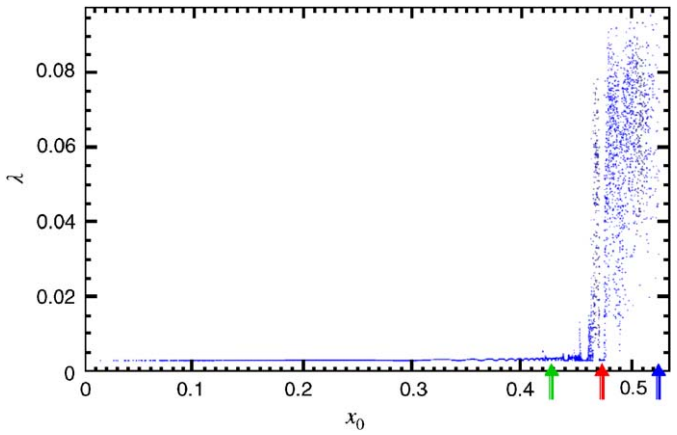

Fig. 1. Standard Lyapunov exponents λ of 10,000 orbits vs. initial condition x_0 ($\dot{x}(0) = 0$ for every orbit), with tune $\eta = 0.15$ and mismatch $M = 0.50$. The localized distributions of the three clumps of Fig. 3 used for mixing experiments with regular orbits (green), 'sticky' chaotic orbits (red), and wildly chaotic orbits (blue) were centered at $x_0 = 0.425$, 0.475, and 0.525, respectively, the latter corresponding to just inside the boundary of the waterbag at $t = 0$. These clumps initially were contained within a length $\Delta x_0 = 0.025$.

then simultaneously propagate all of these test particles according to the equation of motion. We can then measure the volume of phase space spanned by this collection of particles at each time step. A commonly employed measure of phase-space volume is the root-mean-square geometric emittance

$$\varepsilon_g \equiv (\varepsilon_x\varepsilon_y\varepsilon_z)^{1/3}, \quad \varepsilon_i \equiv \sqrt{\langle x_i^2\rangle\langle v_i^2\rangle - \langle x_i v_i\rangle^2}. \tag{6}$$

The procedure of monitoring the evolution of a clump and computing $\varepsilon_g(t)$ is called a 'mixing experiment'. If the clump emittance $\varepsilon_g(t)$ grows exponentially and the clump spreads to a macroscopic region of phase space, 'chaotic mixing' has taken place. In this case the exponential growth rate is a measure of the 'largest Lyapunov exponent' [8–10]. Otherwise, any observed mixing is regular phase mixing, i.e., linear Landau damping [11].

Results of three mixing experiments, one for regular orbits (green), one for 'sticky' chaotic orbits (red), and one for wildly chaotic orbits (blue) appear in Fig. 3. Wildly chaotic orbits are the most likely candidates for halo particles; however, given a sufficient time, sticky chaotic orbits can likewise free themselves and migrate into the halo. Note that *all halo particles pass through the chaotic sea*. When these particles enter a 2:1 resonance with the breathing core (the orbital period being twice the breathing period), the core pumps them to large amplitudes ($|x|_{\max}\sim 4$ with the chosen parameters). However, because the orbital frequency is a function of amplitude, they eventually fall out of resonance and migrate to lower amplitudes. Nonetheless, as we will demonstrate in Section 4 below, these particles can migrate back into resonance and *intermittently* populate the halo. Chaotic orbits eventually mix through the macroscopic phase space accessible to them, whereas regular orbits slowly mix through their relatively localized regular islands. Note that we have scaled the time variable in our figures to the breathing period; this period represents the 'dynamical time' t_D for the waterbag.

The emittances $\varepsilon_g(t)$ ($\varepsilon_g = \varepsilon_x$ for the waterbag) of the three clumps appear in Fig. 2. There are a number of details in these plots, all of which correlate to the evolutionary dynamics exhibited in Fig. 3. (i) The emittance of the wildly chaotic (blue) clump scales exponentially with time, although the exponential growth rate changes value. Initially the growth rate is large as the clump quickly fills the chaotic sea; once the chaotic sea is populated, the growth rate becomes noticeably smaller. It then increases suddenly at the time at which blue orbits begin to enter the halo. Once the halo has a sizable population, the growth rate again becomes smaller. (ii) The emittance of the sticky chaotic clump (red) initially scales as a power law in time, reflecting the initial regularity of these orbits. At time $t\sim 60t_D$, some red orbits start getting unstuck and migrate into the chaotic sea, and the emittance begins to exhibit an exponential scaling. At $t\sim 220t_D$, the emittance jumps up suddenly; red orbits begin entering the halo at this point. The exponential growth rate of the red

clump then settles to a smaller value. (iii) The emittance of the regular clump (green) scales everywhere as a power law in time.

Using the procedure described in Ref. [2], we now incorporate colored noise in the breathing frequency ω (and with our chosen time scale, $\omega = 1$). This noise is unavoidable in real machines; hardware and field irregularities will self-consistently influence the space-charge potential and hence the particle orbits. The noise does work on the beam particles, causing emittance growth and enhanced halo formation. A central finding in Ref. [2] is that, for a homologously breathing, cylindrical, warm-fluid Kapchinskij–Vladimirskij (KV) beam, the outer Kolmogorov–Arnol'd–Moser (KAM) tori are robust; modest noise strength will not break them, although they become *much* more fragile if internal collective modes are excited.

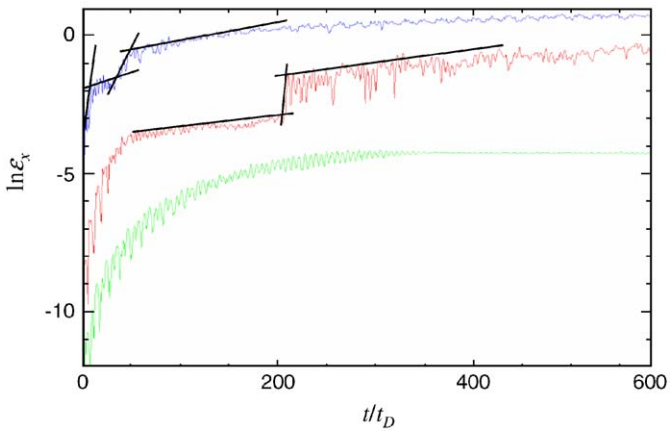

Fig. 2. Plot of $\ln \varepsilon_x$ vs. t for the three clumps of Fig. 3. The lines, which signify exponential scaling of the emittance with time, are meant to guide the eye in following the explanation of the dynamics given in the text.

The influence of noise depends on its strength $\langle|\delta\omega|\rangle$ and autocorrelation time t_c. Taking $t_c = 23t_D$ (as shown in Ref. [2], the exact choice is unlikely to be important), we investigated a broad range of strengths, specifically $10^{-5} \leqslant \langle|\delta\omega|\rangle \leqslant 1$, and found that, just as for the breathing cylindrical KV beam, the outer KAM tori in the stroboscopic Poincaré section of the spherical waterbag are resilient; only very strong noise breaks them. However, a counterexample appears in Fig. 4. These Poincaré sections are derived from sequential computations of 10,000 orbits initially distributed per the waterbag density profile, with noise randomly generated for each orbit separately. In this case, a modest noise strength $\langle|\delta\omega|\rangle = 0.01$ breaks the outer tori and enables particles to leak into a halo having the same dimensions as that of Fig. 3! We also confirmed by mimicking an internal (envelope-matched) mode instead of the breathing (envelope-mismatched) mode that the KAM tori are then much more fragile, just as was true for the aforementioned cylindrical KV beam.

4. Pinpointing orbital chaos

Before applying a new technique for pinpointing orbital chaos in the waterbag, we enumerate certain features of orbital dynamics that are known a priori by virtue of the simplicity of the model. (i) An orbit restricted to the central

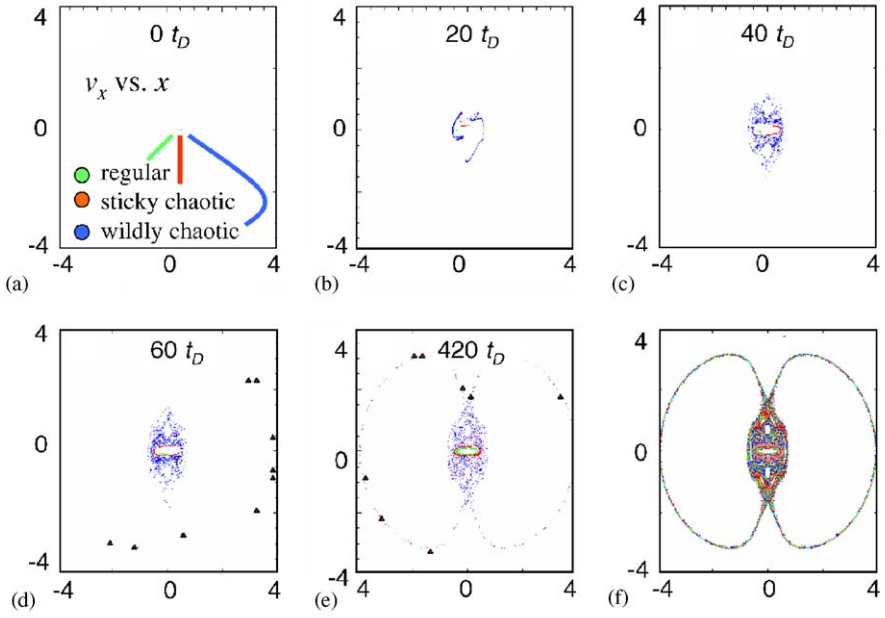

Fig. 3. Stroboscopic Poincaré sections v_x vs. x for the waterbag of Fig. 1. Orbital coordinates are plotted at times for which the waterbag has its minimum radius. Plots (a–e) illustrate evolution of the three clumps, each with 1000 test particles. In plot (d), the triangles flag newly born halo particles. In plot (e), the triangles flag red particles that became 'unstuck' from their regular island, migrated through the chaotic sea, came into contact with the 2:1 resonance, and subsequently populated the halo. Plot (f) shows the complete section computed with 500 test particles that were initially distributed according to the waterbag density profile (the color coding here is arbitrary).

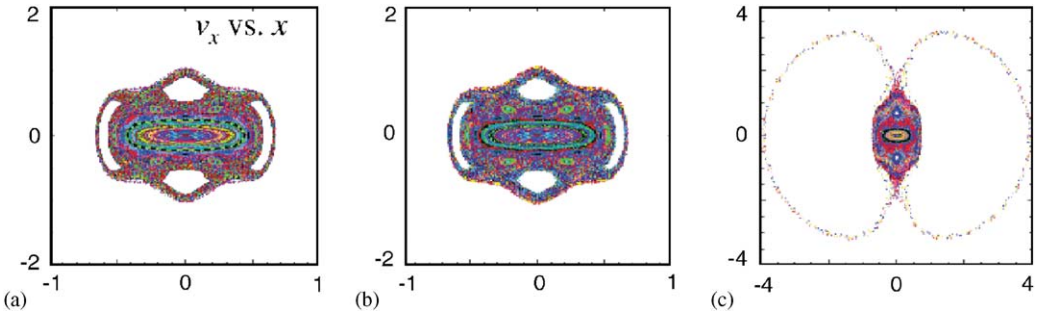

Fig. 4. Stroboscopic Poincaré sections v_x vs. x for the waterbag with tune $\eta = 0.25$ and mismatch $M = 0.5$ and with colored noise strengths $\langle|\delta\omega|\rangle$ of: (a) zero, (b) 0.002, and (c) 0.01. For all cases the autocorrelation time is fixed at $t_c = 23t_D$. Note that in (c) the noise is strong enough to trigger halo formation.

regions of a space-charge-dominated waterbag must be regular. The reason is that the waterbag density is nearly uniform in the central regions; it falls to zero over a relatively short distance near the waterbag's boundary. Thus, the space-charge force acting on a test particle in the interior is linear. This force counters the external focusing force which likewise is linear. In turn, the net force is linear, and the orbit is manifestly regular. (ii) When an orbit is spending time at large amplitudes far outside the waterbag core (such a particle contributes to the 'halo'), it feels predominantly the external focusing force. This force is linear, and an orbit at large amplitude must in turn be regular. (iii) To be injected into the halo, a particle must spend sufficient time near the location of the driving resonance in phase space. The injection process is the 2:1 resonance between the orbital period and the core-oscillation period. The particle enters the core when it is relatively large, such that the retarding space-charge force is relatively small, and then it exits the core when it is relatively small, such that the space-charge kick is relatively large. The core thereby imparts energy to the particle, kicking it to large amplitude. However, the particle cannot stay in 2:1 resonance because its orbital period depends on its amplitude. It will therefore lose energy to the core in the inverse process, and its amplitude will decay. If, however, the particle hovers near the location of the 2:1 resonance in phase space, the entire cycle can repeat without much delay. One would expect a priori that this region of phase space would be chaotic because, e.g., an orbit in this region would be subject to the strongest nonlinearity in the space-charge force. This nonlinearity, added to the time dependence, would seem to be most conducive to chaotic behavior.

With these qualitative considerations in hand, one can set about testing purported measures of chaos for time-dependent systems. Such measures must generate results consistent with these simple expectations. Herein we will test one measure that we have been developing. It is based on orbital dynamics alone. The principal motivation is to characterize efficiently the behavior of orbital epochs and isolate transitions between regularity and chaoticity, and vice versa. Recall that the standard Lyapunov exponent is a time-averaged quantity where the time average is over an infinite interval; hence, it is unsuited to the task. In fact, most of the techniques for characterizing orbits involve the convergence of a measure, whereby the convergence requires a long integration time [12]. This circumstance has motivated alternative methods, most notably frequency analysis [13], that circumvent the need for convergence, but these schemes still require at least tens of orbital periods to yield a reliable characterization. Moreover, all methods devised to date have serious difficulty dealing with sticky orbits (those that are regular for an extended time and then become chaotic) and intermittent orbits (those that transition randomly between regular and chaotic behavior; such transitions may occur quickly and frequently [14]). These are the difficulties we seek to circumvent.

The measure we use devolves from computing an integral of motion I following the method of Struckmeier and Riedel (SR) [15]. For a smooth time-dependent potential $V(\mathbf{x}, t)$, the integral is [16]

$$I = f(t)H - \frac{1}{2}\left[\mathbf{x}\cdot\mathbf{p}\frac{\mathrm{d}f}{\mathrm{d}t} - \frac{1}{2}|\mathbf{x}|^2\frac{\mathrm{d}^2 f}{\mathrm{d}t^2} - c(t)\right], \tag{7}$$

in which H is the Hamiltonian, and the auxiliary function $f(t)$ is the solution of the third-order differential equation

$$\frac{1}{2}|\mathbf{x}|^2\frac{\mathrm{d}^3 f}{\mathrm{d}t^3} + (2V + \mathbf{x}\cdot\nabla V)\frac{\mathrm{d}f}{\mathrm{d}t} + 2\frac{\partial V}{\partial t}f + \frac{\mathrm{d}c}{\mathrm{d}t} = 0,$$
$$f(0) = 1,\ \ddot{f}(0) = \dot{f}(0) = 0,\ \ c(0) = 0. \tag{8}$$

The idea is to solve for the orbit $(\mathbf{x}, \mathbf{p})$ while simultaneously solving for the auxiliary function $f(t)$. The initial conditions are such that $I = H(\mathbf{x}, \mathbf{p}, t = 0)$ for all time. The second auxiliary function $c(t)$ represents a gauge freedom, i.e., $c(t)$ can be chosen for convenience in solving Eq. (8). It can, e.g., be used to remove singularities that would otherwise be present in Eq. (8).

For the waterbag, we choose a gauge $c(t)$ to cancel terms that diverge when the particle passes through the origin, thereby circumventing the respective instability

$$\dot{c} = \left[(\xi R\alpha)^2 - \frac{\zeta}{R}\right]\dot{f} + [2(\xi\alpha)^2 R^3 + \zeta]\frac{\dot{R}}{R^2}f,$$

$$\zeta \equiv (\xi\alpha)^2 + 2\left(\frac{v}{\xi\alpha} - \Delta\right), \quad \Delta \equiv \mu[i_0(\xi) - 1],$$

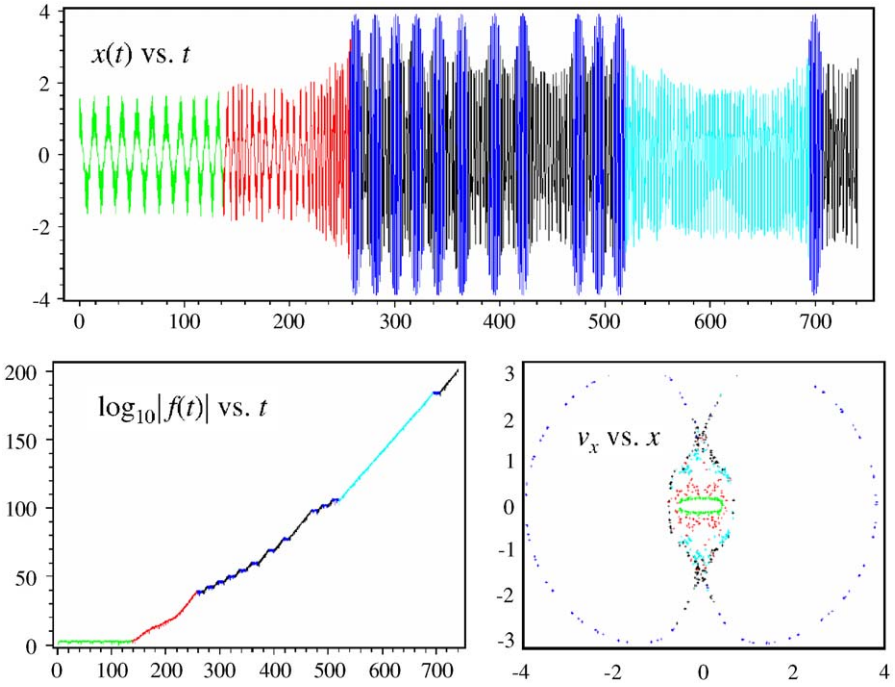

Fig. 5. An example intermittent 'halo orbit' in the waterbag: (top) the trajectory $x(t)$ vs. t; (lower left) $\log_{10}|f(t)|$ vs. t; (lower right) the corresponding stroboscopic Poincaré section. Time is measured in dynamical times (periods of the envelope oscillation). The color scheme is: initial regular epoch (green), initial chaotic epoch (red), regular halo epoch (blue), chaotic halo-to-halo transitions (black), long chaotic 'gap' (cyan).

with which Eq. (8) becomes, after dividing by $x^2/2$:

$$f^{(3)} + 4\left\{\left[1 - \frac{1}{R^3} - \frac{1}{Rx^2}Q\left(\frac{x}{R\alpha}\right)\right]\dot{f} + \left[\frac{3}{2} + \frac{1}{x^2}K\left(\frac{x}{R\alpha}\right)\right]\frac{\dot{R}}{R^2}f\right\}\Theta(\xi R\alpha - |x|) + 4\left\{1 - \frac{1}{2x^2}\left(\frac{\zeta}{R} - \frac{v}{|x|}\right)\dot{f} + \frac{\zeta}{2(Rx)^2}\dot{R}f\right\}\Theta(|x| - \xi R\alpha) = 0 \quad (9)$$

wherein the auxiliary functions $K(y)$ and $Q(y)$ are

$$K(y) \equiv \mu[d_0(y) + j_0(y)] - \Delta,$$

$$Q(y) \equiv K(y) - \frac{\mu}{2}j_0(y), \quad j_0(y) \equiv i_0(y) - \cosh y.$$

The procedure is then to solve Eq. (9) as part of a system of differential equations that includes the equation of test-particle motion.

Consider Fig. 5, which pertains to an orbit that originates well within the beam envelope and eventually gets ejected to large amplitudes. We plot there the orbit itself, the auxiliary function $\log_{10}|f(t)|$ vs. t, and the stroboscopic Poincaré section. At early times, the orbit lingers in the deep interior where the waterbag density is nearly uniform, and in turn the orbit is regular (that $\log_{10}|f(t)|$ plateaus is the signature of regularity). It stays regular for a considerable time and hence is 'sticky'. It gets 'unstuck' and migrates toward the 2:1 resonance with the breathing oscillation; it becomes chaotic during this migration (that $\log_{10}|f(t)|$ grows is the signature of chaoticity). Eventually the resonant coupling becomes strong enough to eject the particle to large amplitudes, whereupon it becomes regular ($\log_{10}|f(t)|$ plateaus). There is a 'beating' at this stage as the orbit intermittently falls out of, then back into, resonance. When out of resonance, the orbit spends most of its time close to the outer region of the chaotic sea where it can migrate back toward resonance, and the orbit is thus again chaotic ($\log_{10}|f(t)|$ grows). However, there is one particularly long chaotic 'gap' between successive halo epochs, which is colored cyan in Fig. 5. The stroboscopic Poincaré section makes clear that during this epoch the orbit 'falls into' the chaotic sea and spends considerable time there before returning to the outer region of the chaotic sea and falling back into 2:1 resonance. We have thereby quantitatively verified that (i) this measure of chaos correctly uncovers the anticipated qualitative physics of the model, and (ii) it teaches us details about the halo-formation process. One sees that $\log_{10}|f(t)|$ gives a crisp, correct, and virtually *immediate* indication of transitions between regular behavior and chaotic behavior.

5. Summary and prospects

Using a simple breathing sphere, a $(1 + 1/2)$-dimensional model, we showed clearly that time-dependence can generate a population of chaotic orbits in nonequilibrium space-charge-dominated beams. We also showed that orbits ejected into a beam halo pass through a chaotic epoch en route to the halo. Such an orbit may populate the halo intermittently, in which case its dynamics is

complicated. However, by applying a new measure of chaos, we dissected the orbital behavior in detail. Moreover, we showed that the presence of colored noise can accentuate halo formation by breaking the outer KAM tori. This is usually more difficult to do for a breathing beam than for a beam with internal space-charge modes; however, we also found that, for certain parameter choices, modest colored noise can nonetheless make a big difference in the macroscopic properties of the purely breathing beam, to include triggering halo formation where otherwise there would be none. The examples chosen herein all carry strong space charge, i.e., a small space-charge-depressed tune, and a strong mismatch. Yet, even with weak space charge, small-amplitude collective modes, and weak noise strength, a pronounced halo is seen to develop if these phenomena act on the beam over a sufficiently long time, such as in a synchrotron or storage ring [17].

Although the spherical waterbag proves very useful for our purposes (illustrating the phenomenology of halo formation and for testing tools for diagnosing chaos), it should not be taken too seriously as a model of a real beam. In a real beam, free energy from mismatch will mix through the hierarchy of scales, causing the beam to settle into a relatively quiescent state (unless, of course, the beam is subject to repeated mismatches). Many 'modes' will be involved, and the 'mode spectrum' will evolve. Moreover, a real beam is a higher-dimensional system. However, one would expect higher-dimensional systems to exhibit the same qualitative behavior that we found with the simple low-dimensional model. The measure of chaos that we used has been successfully tested in higher-dimensional systems as well [16], and it can be implemented in full N-body simulations. Thus, the necessary tool for extracting the detailed microdynamics of nonequilibrium beams appears to be at hand. The anticipated end-product of this measure, or of any other efficient measure (cf., Ref. [18]), is a phase-space microscope with which to monitor the onset and evolution of instabilities, most notably ones that are triggered on a local scale. By integrating all of the initial conditions comprising the system and dissecting the behavior of each respective orbit, one can color-code each orbit at every time step, the color signifying whether it is regular or chaotic at that time, and thereby make high-resolution movies of the evolving phase space of the system. Such movies will not only aid in understanding the fundamental nonlinear dynamics of evolving beams, but also they will enable precise comparisons of the output of different codes.

References

[1] C.L. Bohn, I.V. Sideris, Phys. Rev. ST Accel. Beams 6 (2003) 034203.
[2] I.V. Sideris, C.L. Bohn, Phys. Rev. ST Accel. Beams 7 (2004) 104202.
[3] R. Balescu, Statistical Dynamics, Imperial College Press, London, 1997.
[4] H.E. Kandrup, I.V. Sideris, C.L. Bohn, Phys. Rev. ST Accel. Beams 7 (2004) 014202.
[5] T.P. Wangler, K.R. Crandall, R. Ryne, T.S. Wang, Phys. Rev. ST Accel. Beams 1 (1998) 084201.
[6] H. Okamoto, M. Ikegami, Phys. Rev. E 55 (1997) 4694.
[7] R.L. Gluckstern, A.V. Fedotov, Phys. Rev. ST Accel. Beams 2 (1999) 054201.
[8] C.L. Bohn, in: J. Rosenzweig, L. Serafini (Eds.), The Physics of High-Brightness Beams, World Scientific, Singapore, 2000, pp. 358–368.
[9] H.E. Kandrup, I.V. Sideris, C.L. Bohn, Phys. Rev. E 65 (2002) 106214.
[10] C.L. Bohn, I.V. Sideris, Phys. Rev. ST Accel. Beams 6 (2003) 034203.
[11] D. Sagan, Am. J. Phys. 62 (1994) 450.
[12] G. Contopoulos, Order and Chaos in Dynamical Astronomy, Springer, Berlin, 2002.
[13] J. Laskar, Icarus 88 (1990) 266.
[14] H.E. Kandrup, I.M. Vass, I.V. Sideris, Mon. Not. Roy. Astron. Soc. 341 (2003) 927.
[15] J. Struckmeier, C. Riedel, Phys. Rev. Lett. 85 (2000) 3830.
[16] C.L. Bohn, B. Terzić, Phys. Rev. E, submitted for publication.
[17] C.L. Bohn, AIP Conf. Proc. 737 (2004) 456.
[18] I.V. Sideris, Ann. NY Acad. Sci. 1045 (2005) 79;
I.V. Sideris, Phys. Rev. E, submitted for publication.